Four years of good SpeX

John T. Rayner[a], Peter M. Onaka and Michael C. Cushing[b]
University of Hawai'i, 2680 Woodlawn Drive, Honolulu, HI, USA 96822

William D. Vacca
NASA Ames Research Center, MS 144-2, Moffet Field, CA 94035

ABSTRACT

SpeX is a cross-dispersed medium-resolution 0.8-5.5μm spectrograph in operation at the NASA Infrared Telescope Facility (IRTF) on Mauna Kea, Hawaii. The instrument uses prism cross-dispersers and gratings to provide resolving powers up to R~2000 simultaneously across 0.8-2.4μm or ~2-5.5μm. An autonomous infrared slit-viewer is used for object acquisition, guiding, and scientific imaging. The spectrograph employs a 1024x1024 Aladdin 3 InSb array and the imager a 512x512 Aladdin 2 InSb array. Since it was commissioned in June SpeX, has been used for about 45% of all telescope time. We give an overview of the design, followed by details of the use and performance of the Aladdin arrays, observing techniques, maintenance issues, and lessons learned.

Keywords: infrared instrumentation, infrared spectrograph, infrared guider, infrared arrays

1. INTRODUCTION

SpeX is cross-dispersed medium-resolution 0.8-5.5μm spectrograph in operation at the NASA Infrared Telescope Facility on Mauna Kea. The design, construction, and initial performance of SpeX are discussed in Rayner *et al*.[1] In this paper we discuss four years of operational experience with SpeX. In particular, we discuss issues related to the use of Aladdin arrays and observing techniques, which might be of interest to observers and instrument builders, followed by a brief discussion of maintenance issues and lessons learned.

2. INSTRUMENT OVERVIEW

The cryostat is mounted at the Cassegrain focus of the telescope by a rigid interface box, into which is built a spectral calibration unit consisting of transfer optics, an integrating sphere, flat-field lamps, and an arc lamp. Three sections make up the cold optics: the fore-optics, the infrared slit-viewer/guider, and the spectrograph. A photograph of SpeX mounted to the telescope is shown in Figure 1. The optical layout and internal view of the cryostat is shown in Figure 2. Cooling is done with a two-stage 1050-CTI cooler and a liquid nitrogen can. The liquid nitrogen can cools the cold structure to an operating temperature of 80 K in two days. The first stage of the cooler cools a radiation shield and the second stage operates the detectors at 30 K.

In the fore-optics, the f/38.2 beam entering the cryostat window first encounters a dichroic turret before coming to a focus. Visible-reflecting/infrared-transmitting dichroics feed the visible beam to an optical wavefront sensor package mounted on the side of the cryostat. The optical path following the cold telescope focus comprises a collimating mirror, fold mirrors, an order sorter filter wheel, a 12.5 mm cold stop, a K-mirror image rotator, and a camera lens. This system re-images a 60x60 arcsec field of view onto a slit wheel and feeds an f/12.7 beam into the spectrograph.

The field surrounding the slit is reflected into the slit-viewer by a slit-mirror. The slit-viewer consists of a collimating lens, a 12.5 mm cold stop, a filter wheel, a camera lens, and an array. A 60x60 arcsec field is re-imaged onto a 512x512 Aladdin 2 InSb array, giving an image scale of 0.12 arcsec/pixel. In addition to object acquisition and scientific imaging, the slit-viewer is used for infrared guiding on either spill-over light from the science object in the slit or on an object in the field.

[a] Email: rayner@ifa.hawaii.edu
[b] Current address: SETI Institute, NASA Ames Research Center, MS 245-3, Moffet Field, CA 94035

The f/12.7 beam entering the spectrograph is first folded before collimation by an off-axis parabola. The collimator forms a 24 mm diameter image of the telescope pupil on a grating/prism mounted in a grating turret wheel. Following dispersion, a camera lens images the spectrum onto a 1024x1024 Aladdin 3 InSb array, which is mounted on a focusing stage. The spatial scale is 0.15 arcsec/pixel. Because of the wide wavelength range, cross-dispersion is done with prisms, which are used in double-pass mode. To keep the spacing of the cross-dispersed orders equal, which is essential to maximize slit length, different prism materials are used depending on wavelength; a fused silica/ZnSe dual-prism is used in the 0.8-2.4 μm mode, and a LiF/germanium dual-prism is used in the 1.9-5.4 μm mode. The grating turret has five positions: two grating/prism cross-dispersed modes, two grating long-slit modes, and one low-resolution prism mode. All the lenses are BaF_2-LiF-ZnS/Cleartran achromatic triplets, antireflection coated for 0.8-5.5 μm.

An IRTF-designed array controller runs both the spectrograph and imaging InSb arrays. Cryostat-mounted electronics, consisting of preamps, analog to digital boards, clock, and bias boards, are fiber-optically coupled to the array controller, which resides in the telescope control room. The optical fibers are 100 m long. The VME64-based array controller uses digital signal processor (DSP) boards (each containing four DSPs), and a single-board SPARC computer. One controller ("Bigdog") runs the spectrograph array, and a second ("Guidedog") runs the slit-viewer array. A PC-based instrument computer ("Littledog") mounted on the mirror cell is used for motor and temperature control, and for monitoring tasks. A graphical user interface (GUI) runs on a two-screen Unix workstation connected to the array controller and instrument computer by Ethernet.

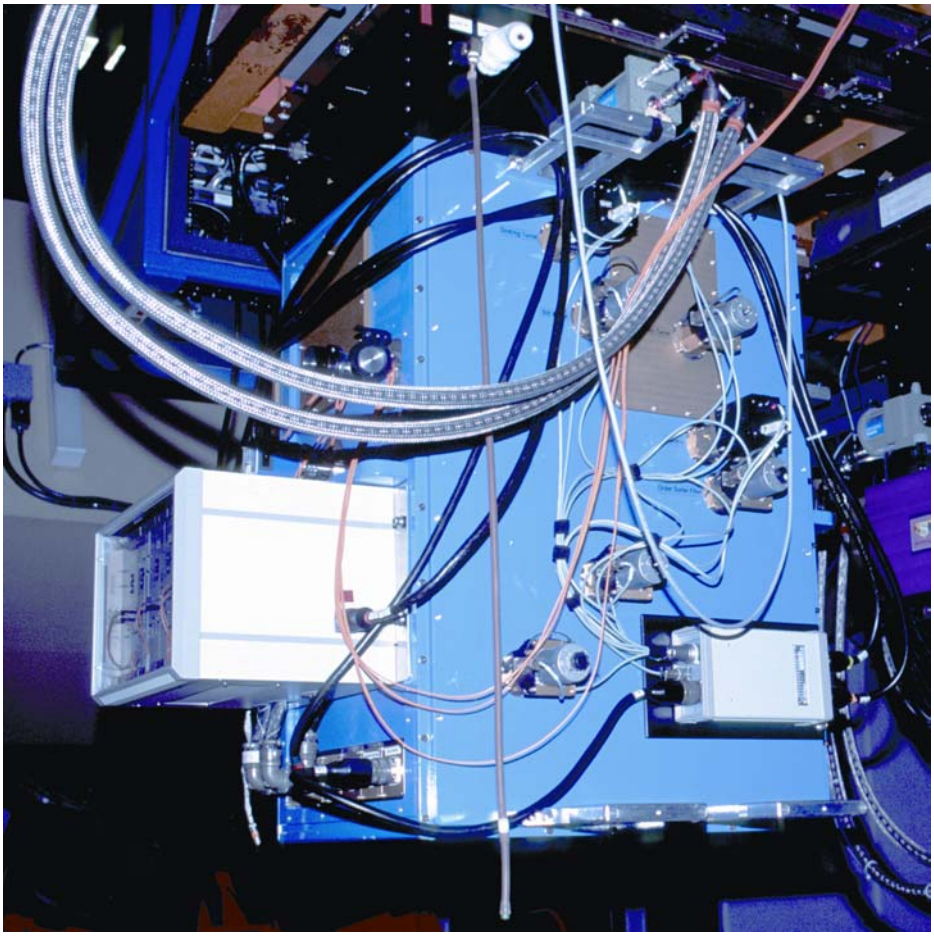

Figure 1 Photograph of SpeX on IRTF. The cryostat (blue box) is mounted to the telescope by the black interface box which contains the spectral calibration unit. The closed-cycle cooler is visible at the top of the cryostat. Visible on the front cover of the cryostat are motors for controlling the seven internal mechanisms. Mounted to the side of the cryostat to the lower left is the electronics box containing clock, bias, preamp, analog-to-digital, and fiber-optic boards. For scale SpeX is 1.4m tall and weighs 478kg.

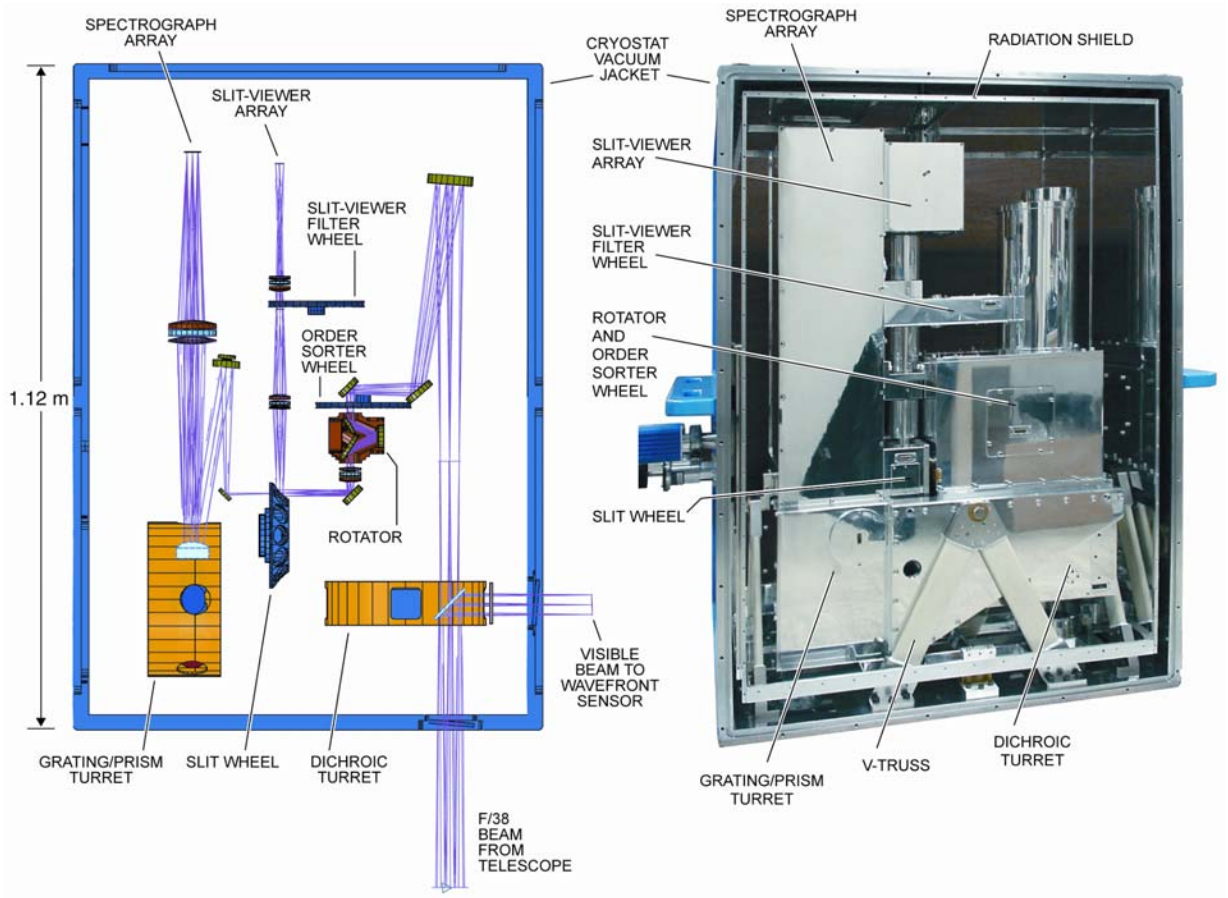

Figure 2 *Left*: Optical layout of the cryostat. *Right*: Photograph of the vacuum jacket and cold structure, shown with the front and back covers of the cryostat removed. Immediately inside the vacuum jacket is the closed-cycle cooled radiation shield, also shown with the covers removed. The cold structure is mounted to the vacuum jacket by four fiberglass V-trusses. The interior is highly polished to reduce emissivity without the need for multi-layer insulation.

3. OPERATIONAL EXPERIENCE WITH ALADDIN ARRAYS

3.1 General properties and read out methods

SpeX uses a science grade 1024x1024 Aladdin 3 InSb array in the spectrograph and an engineering grade 512x512 Aladdin 2 InSb array in the slit-viewer/guider. The arrays are read out using multiple correlated double sampling (MCDS[2]). In CDS the procedure is to reset each pixel to the reverse bias voltage, read the pedestal voltage, and then read the signal voltage after a nominal integration time. In MCDS the pedestal and signal levels are read multiple times to reduce the readnoise. (Each correlated double sample is also known as a non-destructive read or NDR - a correlated pair of reads.) Two options are available for resetting the array, global resets or pixel-by-pixel resets. In pixel-by-pixel resets the reset to pedestal read interval is fixed. In global resets this interval varies with pixel and results less uniformity of response. A global reset resets all pixels at the same time and is faster than the sequential pixel-by-pixel reset. Global resets are used in SpeX because they allow much shorter integration times and therefore increase the dynamic range of the instrument, while the uniformity is still acceptable. The global reset pulse is optimized at 20 μs. If the reset pulse is shorter electronic ghost images result while longer resets increase image persistence and thermal effects (as discussed below).

A summary of the basic array performance characteristics are given in Table 1. Both the spectrograph and guider arrays are operated at a reverse bias of -0.4 V. The choice of reverse bias is a trade-off between well depth and noise. Larger biases give more well depth but at the cost of higher dark current and readnoise. To speed the read out process all 32 outputs (8 per quadrant) of the spectrograph array are read out in parallel. Similarly all 8 outputs of the (one quadrant) guider array are read out in parallel.

Parameter	**Spectrograph**	**Slit Viewer/Guider**
Detector	1024x1024 Aladdin 3 InSb	512x512 Aladdin 2 InSb
Gain	12.1 $e^- DN^{-1}$	14.7 $e^- DN^{-1}$
Saturation level (0.4 V rev. bias)	~8500 DN	~6000 DN
Recommended range (0.4 V rev. bias)	<4000 DN (~10% linear)	<2500 DN (~10% linear)
Read Noise	47 e^- RMS with 1 NDR	60 e^- RMS with 1 NDR
	15 e^- RMS with 32 NDRs	20 e^- RMS with 32 NDRs
Dark current	0.2 $e^- s^{-1}$	1.5 $e^- s^{-1}$
Persistence current 1000 DN	~1 $e^- s^{-1}$	
2000 DN	~3 $e^- s^{-1}$ decay time constant 2-10 min	
3000 DN	~7 $e^- s^{-1}$ decay time constant 2-10 min	
4000 DN	~14 $e^- s^{-1}$ decay time constant 2-10 min	
Readout rate full array (standard)	0.51 s per NDR	0.24 s per NDR
Readout rate full array (fast)	0.1 s per NDR	0.12 s per NDR

Table 1 Summary of array parameters

3.2 Readnoise and duty cycle

During readout the dwell time per pixel is controlled by a parameter called slow-counts (the number of no operations). With slow-counts set to 20 the minimum full array read out time is 0.51 s per NDR (equal to the minimum on-chip integration time) and the resulting readnoise 47 electrons RMS for the spectrograph array. This is the default mode for spectroscopy. With slow-counts set to 2 the minimum full array read out time (and on-chip integration time) is reduced to 0.1 s per NDR but the readnoise increases to about 60 electrons RMS. The increased readnoise is not significant when short on-chip integration times are used, for example, to avoid saturation on bright objects. However, it is a factor when fast readouts are required, as is the case for occultations, for example. On-chip integration times can be further reduced by using subarray readouts. The number of NDRs (N_R) is increased up to a maximum of 32 as the on-chip integration time (T_C) is increased (to do 32 NDRs requires $T_C > 16.32$ s for the default readout rate of 0.51 s per NDR). Using the spectrograph array, Vacca *et al*.[3] find that effective readnoise decreases as $N_R^{-0.35}$. This is shallower than the theoretical rate of $N_R^{-0.5}$ but the improvement is still significant (see Table 1). The disadvantage of performing NDRs is the overhead required to do the extra reads. For a given on-chip integration time the instrument control software selects the maximum allowable number of NDRs up to a maximum of 32. However, if observers wish to optimize for either readnoise or observing efficiency the number of NDRs can be selected manually.

3.3 Correcting for nonlinearity

The detection process in infrared arrays is inherently nonlinear because detector capacitance is discharged during integration as photons are detected. The SpeX arrays are operated in the lower 50% of the useable detector well depth (counts < 4000 Data Numbers (DN)) since this is where the response is most linear. However, even here if nonlinearity is not taken into account source flux can be underestimated by ~10%. When applying a correction for nonlinearity to data acquired with MCDS, correction must be made to both the signal and pedestal levels separately and not to net source counts (signal minus pedestal). This is because the time between the reset and pedestal read is fixed and the detector continues to integrate flux during this interval. Consequently the absolute position of the pedestal is a function of source flux, the brighter the source the higher the pedestal in the well. However, MCDS does not record separate pedestal and signal levels, only signal minus pedestal. A procedure developed by Vacca *et al*.[3] uses an estimate of the source flux to iteratively converge on the absolute levels and applies the correction for nonlinearity to the absolute levels. An example of both the necessity of correcting for nonlinearity and the effectiveness of the procedure developed

is seen in Figure 3, which is taken from the paper by Cushing *et al.*[4]. This figure shows spectra in adjacent spectral orders, where the flux in the raw images is significantly different due primarily to grating blaze effects. Spectra reduced without correction for nonlinearity do not match in either intensity level or spectral slope in the overlapping wavelength region. After applying correction for nonlinearity, however, the spectra agree both in intensity and slope to better than a few percent over the entire overlap region.

3.4 Dark current and persistence

An operating temperature of 30 K was found to be the best compromise between dark current, which increases with temperature, and readnoise, which decreases with temperature. The blanked-off median dark current of the spectrograph and guider arrays is 0.2 $e^- s^{-1}$ and 1.5 $e^- s^{-1}$, respectively. Unfortunately the low dark current performance of the spectrograph array, which is required for the best spectroscopic performance, is largely negated by image persistence effects. Image persistence acts like dark current with the additional property that it decays with a characteristic time

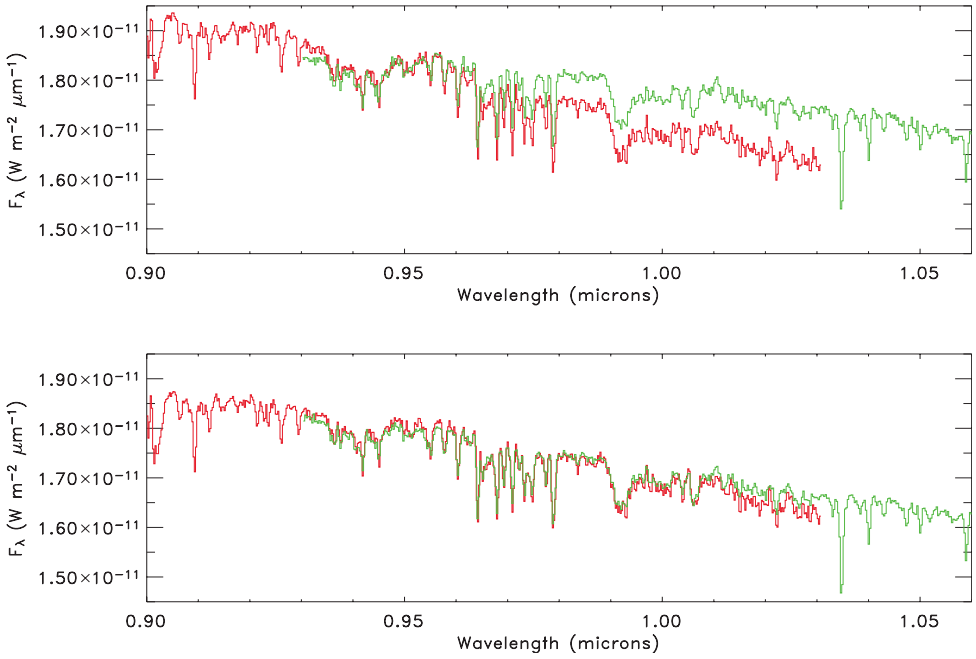

Figure 3 Spectra of Gl 846 (M0.5 V) from cross dispersed orders 6 and 7 of the SXD mode. The spectra were reduced using the *Spextool* reduction package (Cushing et al. 2003) without (upper panel) and with (lower panel) correction for nonlinearity. Correction for nonlinearity largely removes the mismatch in both flux levels and slope of the spectra in the overlap region. No additional scaling has been applied to these spectra**.**

constant, following exposure to flux. For this reason we will refer to it as persistence current. Typically, persistence current is greater than an order of magnitude higher than dark current. Table 1 gives the persistence current as a function of the brightness level in the previous exposure, measured immediately following with a 60 s blanked-off integration. A variety of techniques were tested to reduce the effects of persistence including zeroing the bias and taking flush images. We found that the most effective procedure is to run continuous global resets at 2 Hz with a 40 μs reset pulse when the arrays are otherwise idle in between exposures. The reset pulse is adjusted to 20 μs immediately prior to taking an exposure. Operating the arrays in this manner reduces the persistence current by about a factor of four. The decay time constant for persistence current is a about two minutes for the first few minutes, lengthening to five minutes after about five minutes, and to 10 minutes after about 20 minutes. The time constant is independent of running continuous global resets. One disadvantage of running continuous global resets in between exposures is that the bias level changes and is no longer spatially flat when long exposures are first started. The result is that the first object minus sky pair subtraction is not spatially flat. This might be due to thermal effects as heat dissipation in the array multiplexer is reduced when switching from continuous resets to a more quiescent state during long exposures. However, the effect is small and it is not apparent after the first pair of an exposure sequence.

3.5 Image artifacts

Two other types of artifacts appear spatially and temporally at random in spectral images. The first are circular features of negative bias typically in the range of 0-10 DN deep and on average 25-50 pixels in diameter. We believe these artifacts can result from temperature instability in the array since careful optimization of the proportional (P), integral (I) and differential (D) coefficients of our Lakeshore 330 temperature reduces their frequency. These artifacts also become less frequent once the arrays have been under vacuum and cold for a few weeks. Under these conditions occurrences in the spectrograph array are rare (less than one or two events per hour of total integration time). The second type of artifact is clusters of bright pixels. These are always 3-4 pixels in diameter with the central pixels close to saturation (>5000 DN). They appear on average once every 10 s. Almost identical features and occurrences (scaled for array area) are seen in the 256x256 InSb array in the IRTF's echelle spectrograph, CSHELL. This would appear to eliminate the possibility we considered that the events in SpeX are due to radioactive decay of ThF_4 used in the anti-reflection coatings of the SpeX refractive optics since CSHELL uses reflective optics and contains no ThF_4 coatings. We conclude that the bright pixel clusters are caused by cosmic rays. The significance of these artifacts to observers is that in some observing modes it might be better to median together several images rather than take a couple of long exposures, even though the longer exposures might in principle result in a better signal to noise ratio by integrating longer to become background limited rather than readnoise limited. Both artifacts are too big to be fixed by post observation interpolation should they fall upon spectra. A few tens of 'hot' pixels also appear at random in spectral images but these are easily fixed by interpolation.

4. OBSERVING TECHNIQUES AND PERFORMANCE

4.1 Infrared guiding

There are two guiding modes available when acquiring spectroscopy with SpeX: off-axis guiding using the IRTF's CCD guider, and on-instrument infrared guiding using the slit-viewer. The slit-viewer images a 60x60 arcsec field centered on the slit and guiding is done on spill-over flux from the science object in the slit or on any suitable sources in the field. In the cross-dispersed modes, guiding can done through any of the filters in the slit-viewer filter wheel. Only in rare cases where the science object is too faint to guide on and there are no other objects visible in the slit viewer field is the off-axis CCD guider needed. There are two main advantages of using the infrared guider over the off-axis visible guider. First, there is no measurable flexure between the slit viewer and the spectrograph since both are mounted to the same rigid cold structure. By comparison flexure between the visible guider and spectrograph can be larger than the slit width. Second, guiding is done at a wavelength closer to, and usually within, the spectral range of the observation. This increases throughput and minimizes spectral slope variations in spectra as discussed in section 4.2.

Figure 4 shows the image display and Figure 5 shows the control widget used by observers to interact with infrared guider. In this example the

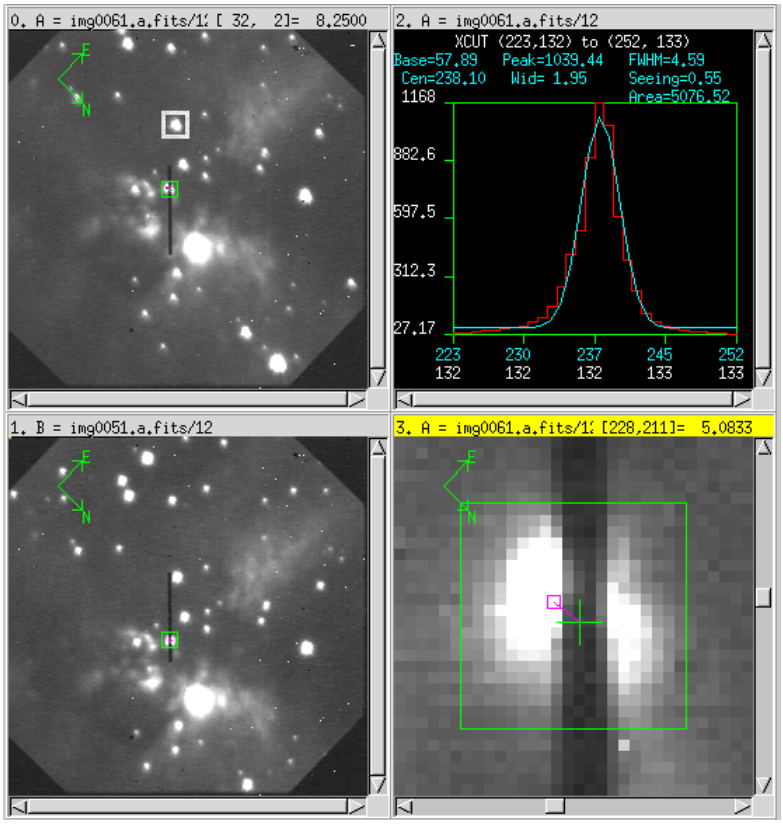

Figure 4 Image display window for the infrared guider.

guider is setup to guide on a point source about 20 arcsec south of BN in Orion. The top-left and bottom-left panels of the image display show the target in the A and B beam guideboxes (green) respectively. In this case the selected slit size is 0.5x15 arcsec. The design slit length is a trade-off between having a shorter slit to fit more cross-dispersed orders onto the spectrograph array, and having a longer to slit allow point source nodding along the slit. Using the internal K-mirror image rotator the position angle (as indicated by the compass) was set to 135 degrees to keep other sources out of the slit. Guiding was done in the K-band where the target has a magnitude of about 9.5 and the guider integration time was 1.0 s with 3 co-additions. The upper-right panel shows an intensity profile cut (full-width-half-maximum 0.55 arcsec) through the star in the white in the upper-left panel. The lower-left panel shows the realtime display of the target in the guidebox. The guidebox is 30 pixels square and the image scale is 0.12 arcsec per pixel. A green cross marks the center of the guidebox and the small purple box the calculated centroid of the flux spilled over from the target. The telescope is offset to center the target in the slit.

The guider setup GUI is shown in Figure 5. Clicking on 'Auto GuideBox Setup' selects the default guidebox coordinates and sizes for a given slit and also sets up the telescope nod for a given position angle. Other guidebox positions and sizes can be entered manually. Guider parameters prefaced by an asterisk may be changed on-the-fly to fine tune guiding. The best guide algorithm employs simple centroiding of the flux inside the guidebox. Guiding works well both on point sources and extended objects such as planetary disks and galactic nuclei, and even centrally saturated point sources. In 'Slow Guide' mode corrections are done by simply offsetting the telescope at a rate of 1 Hz and slower. (A 'Fast Guide' mode using the telescopes tip-tilt secondary has not been implemented.) The amount of the calculated guide correction used to offset the telescope is controlled by the gain parameter. For bright targets setting the gain to less than one avoids oscillating about the slit (positive feedback) which can sometimes result when guiding on image speckles. Lengthening the integration time (by increasing coadds) to a couple of seconds to smear out the speckles also helps in this regard. Other methods used to improve guiding include subtracting a stored sky image when the target is faint compared to the sky. This is particularly useful for guiding on faint red objects in the *K*- and *L*-bands. It has not been found necessary to flat-field guide images, however, 'hot' pixels are flagged and are not included in centroid calculations since they can significantly perturb corrections on faint targets.

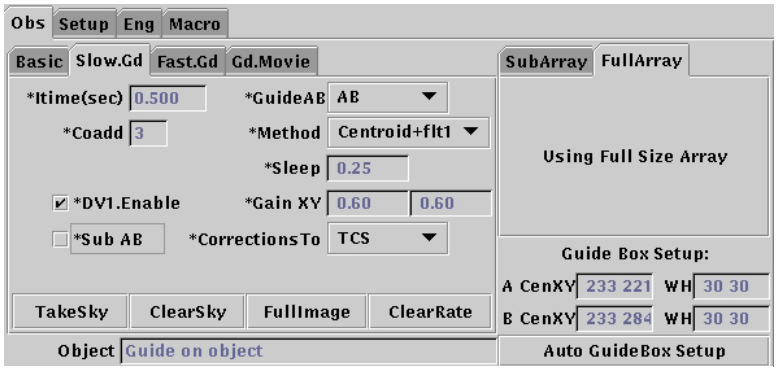

Figure 5 Infrared guider control widget from the guider GUI.

Brightness limits for guiding are dependent upon filter, slit width, integration time, and seeing conditions. As an example, when guiding on spill-over light from a point source science target in the slit, auto-guiding works down to a magnitude of about 15 in the *J*-band filter for a slit width of 0.5 arcsec and a guider on-chip integration time of about 15 s in median seeing conditions of about 0.7 arcsec. Under the same conditions manual guiding using the image display works down to a magnitude of about 18 at *J* band, on a point source in the slit, while auto-guiding at *J* band on a point source in the field works down to a similar magnitude.

4.2 Spectroscopy at 0.8-2.5 µm

Three spectroscopy modes are available in the 0.8-2.5 µm wavelength range: 0.8-2.4 µm spectroscopy in six cross-dispersed orders (R=2000 matched to a slit width of 0.3 arcsec), single-order 60 arcsec-long-slit spectroscopy, and 0.8-2.5 µm prism spectroscopy (R~250 matched to a slit width of 0.3 arcsec). In this wavelength regime the sky background is very low in between the OH lines (~0.015 $e^- s^{-1}$ $pixel^{-1}$)[1] and spectroscopy (R~1000-2000) using Aladdin arrays is array limited (due to readnoise and persistence current) and not sky background limited. With a nominal persistence current ~1e/s on-chip integration times of about 300 s are adequate to overcome readnoise in the background limit which is set by persistence. Longer integration times are avoided since it is better to median several images together to remove the image artifacts discussed in section 3.5. The prism mode is sky background limited over most of its wavelength range in 300 s due to its lower spectral resolution.

In principle infrared spectral images can be obtained and reduced much like CCD spectral images: (A - dark)/flat-field, where A is the telescope A beam or object image. The dark image is usually not taken at the time of the observation since it is stable and can therefore be acquired at a more convenient time. Even though the infrared sky background can be higher and more variable than in the optical, a separate sky image is not required since the sky can be subtracted by fitting along the slit, provided the object does not fill the length of the slit. However, when using SpeX the procedure is (A -B)/flat-field, where B is a sky image of the same exposure time as A obtained by nodding the source along the slit. The reason for taking a nodded image immediately following the object image is to subtract to first order time variable effects, particularly persistence current. With point sources there is no loss in efficiency taking sky images since point sources can be nodded in the slit.

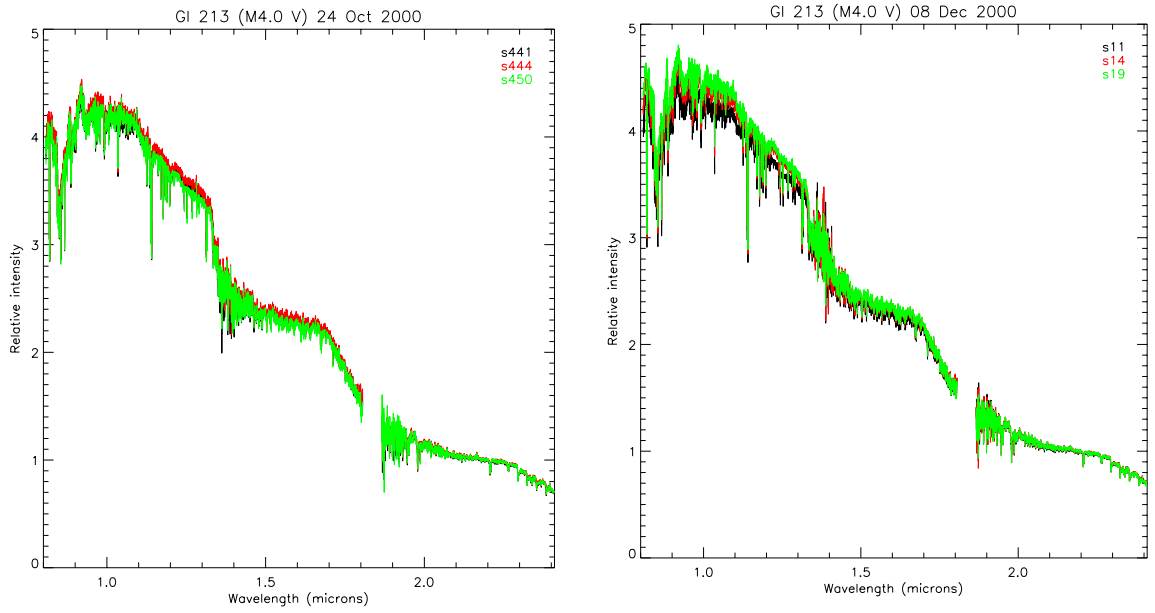

Figure 6. *Left.* Three consecutive spectra (black, green and red) of Gl 213 from 24 Oct 2000, taken with the slit at the parallactic angle. *Right*: Three consecutive spectra of Gl 213 from 08 Dec 2000, taken with the slit not at the parallactic angle. The seeing was about 0.8 arcsec at K on both nights. Both objects were observed at an air-mass of 1.1. Observing at the parallactic angle reduces spectral slope differences.

Aside from the overall gain in efficiency attained through cross dispersed spectroscopy one of the expected advantages is the precision of the measured spectral shape compared to piecing together spectra taken in single orders. However, due to the wavelength and time dependent effects of seeing, atmospheric refraction, and guiding, on the PSF, slit throughput is a function of wavelength and time. Consequently, spectral shape cannot be measured perfectly. Goto *et al.*[5] have observed and modeled these effects in AO spectroscopy. In Figure 6 we give examples of spectral shape variations in the seeing limited case. In general we find that slope variations are minimized by observing at the parallactic angle. The position angle of the slit is aligned with the parallactic angle using the K-mirror rotator. At best individual spectra taken over periods of several minutes show slope variations of about 2% of the flux across the 2.5 μm baseline (i.e. if the spectra are normalized at 2.4 μm the flux of individual spectra vary by 2% at 0.9 μm). However, spectra not observed at the parallactic angle can show much larger slope variations. The example shown in Figure 6 has a slope variation of about 7% of the flux across the 2.5 μm baseline.

As an illustration of the wavelength and time dependence of the PSF (strictly speaking, the FWMH along the slit), Figure 7 plots the FWHM as a function of wavelength measured in prism spectra of standard stars taken two different nights. The night of 25 January 2001 shows a weak wavelength dependence of $\lambda^{-0.21}$, very close to the $\lambda^{-0.20}$ dependence of Kolmogorov turbulence. Over the course of several minutes the exponent varied between -0.21 and -0.15. The FWHM is dominated by seeing but includes a contribution from guiding. The night of 22 March 2001 shows a slightly stronger wavelength dependence of $\lambda^{-0.32}$ and overall a smaller FWHM.

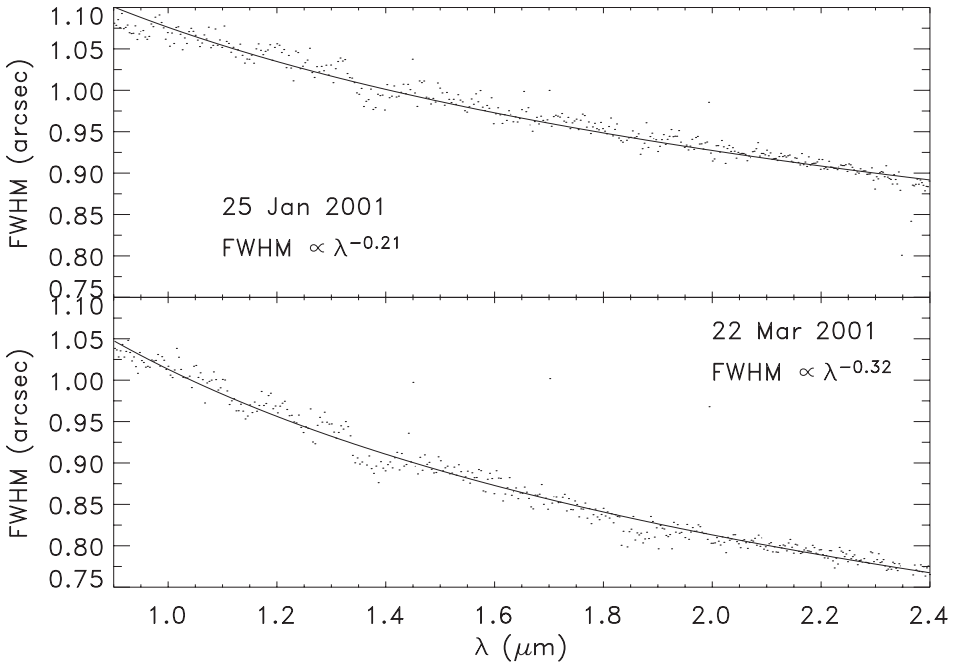

Figure 7 Plots of full FWHM versus wavelength extracted from 0.8-2.5 μm prism spectra of standard stars. The FWHM is dominated but seeing but includes a contribution from guiding.

4.3 Spectroscopy at 2-5.5 μm

Two spectroscopy modes are available in the 2-5.5 μm wavelength range: 2.4-5.4 μm spectroscopy in five cross-dispersed orders (R=2500 matched to a slit width of 0.3 arcsec), and single-order 60 long-slit spectroscopy. With small rotation adjustments to the grating turret the ranges 1.9-4.2 μm and 2.2-5.0 μm can also be covered in six orders each. Due to the large increase in thermal background from the sky and telescope across 2-5 μm, and the broad wavelength grasp of the cross dispersed mode, spectra are typically background limited at long wavelengths ($\lambda > \sim 3$ μm, depending on the on-chip integration time needed to avoid saturation) and readnoise limited at short wavelengths ($\lambda < \sim 3$ μm). However, except for very red sources, most observing programs are source-limited at 2 μm because of the finite source brightness required for detectability at 4-5 μm. (A notable exception is T dwarfs). To prevent saturation on-chip integration times are limited to about 60 s at 4.0 um and about 5 s at 5.0 μm for the 0.3 arcsec-wide slit. We have found that spectral extraction is improved by obtaining good sky subtractions. Due to sky variability in this wavelength range telescope nods are made at least once every minute in good conditions.

Relative to 0.8-2.5 μm, observing at 2-5.5 μm is strongly affected by atmospheric conditions, principally cirrus and water vapor content. At shorter wavelengths the effect of cirrus is to reduce signal. However, at longer wavelengths cirrus can significantly increase sky noise by reflecting higher temperature ground radiation into the beam since the effective sky temperature is much lower than the ground. This coupled with the decrease in signal through absorption makes the effect of cirrus on signal-to-noise more severe at thermal wavelengths.

In the 0.8-5.5 um range there strong and broad telluric absorption features at ~1.1 μm (mostly H_2O), ~1.4 μm (mostly H_2O and CO_2), ~1.85 μm (mostly H_2O), ~2.6 μm (mostly H_2O and CO_2), and ~4.3 μm (mostly CO_2). In addition telluric H_2O absorption affects much of the 2.9-3.5 μm and 4.5-5.5 μm 'windows'. Consequently, the water vapor content of the atmosphere can have a strong influence on data quality. To remove telluric features we use the standard technique of dividing the object spectrum by the spectrum of a 'featureless' standard star observed nearby in both air-mass and time. (We use A0 V stars which are made featureless by modeling and removing intrinsic hydrogen absorption lines as described by Vacca *et al.*[5]) In regions of strong and highly structured telluric absorption even small amounts of spectral shift between the object and standard spectra can result in poor removal of telluric features. To minimize the amount of

instrument flexure, the angular distance moved between the between the two observations is also minimized. Any relative shift between the object and standard star spectra can be measured and corrected during data reduction. However, the fidelity of sampling the telluric structure ultimately limits how well it can be removed. We have found that over-sampling spectra (i.e. better than two pixels per slit width) is required for good telluric correction in regions of deep and dense absorption lines. On average the flexure in SpeX is 1-2 pixels going from zenith to 60 degrees over. For typical object-standard star angular separations (~5 degrees) this results in a relative movement of 0.1-0.2 pixels. Figure 8 illustrates how even these small shifts can seriously degrade the quality of spectra in the 3.0-3.4 μm region where telluric absorption lines are deep and dense, if these shifts are not corrected. The *Spextool* reduction package developed by Cushing *et al*.[5] measures any shift between the object and standard spectra using an autocorrelation procedure and shifts spectra prior to division to remove telluric features.

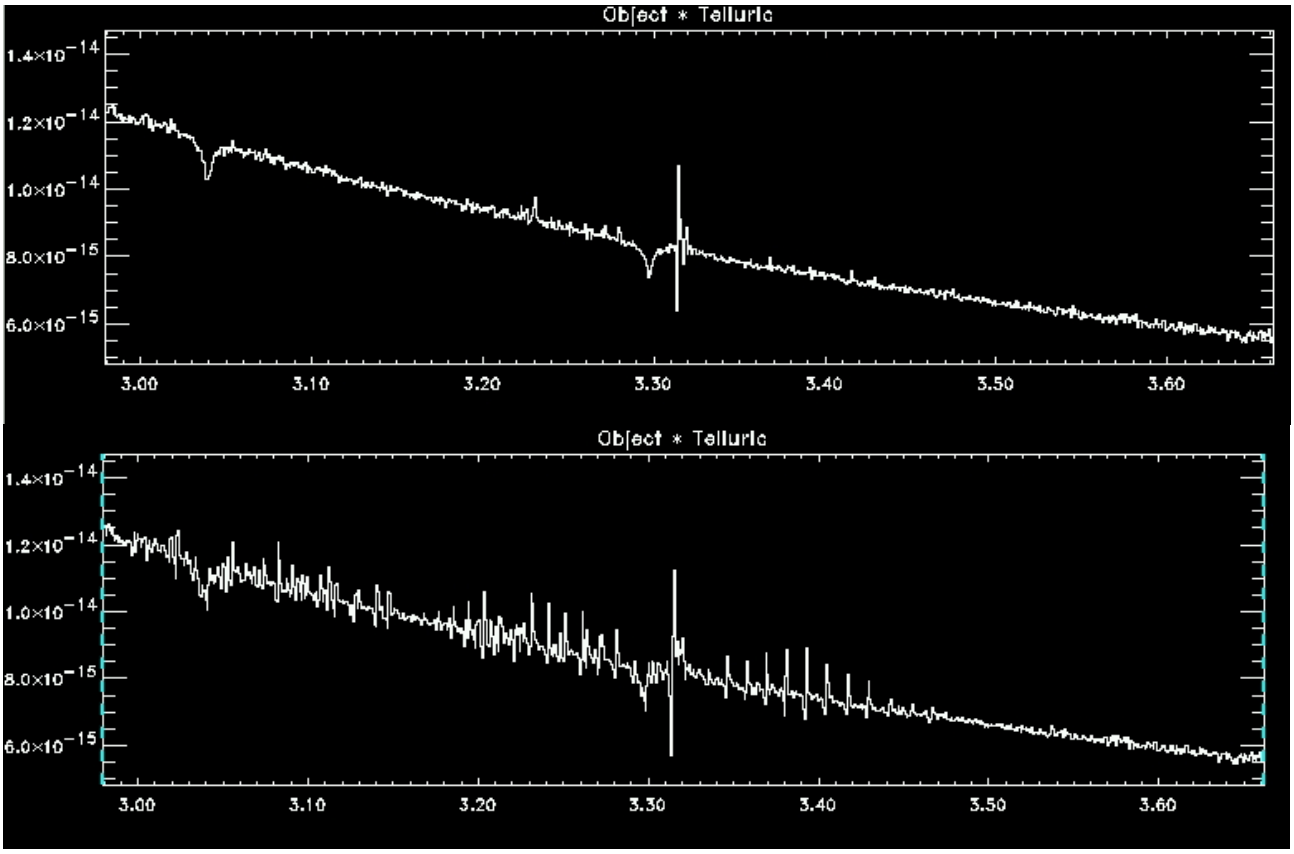

Figure 8 *Bottom*: Spectrum of a B5 V star without correction for a 0.2 pixel (1/10 of the slit width) wavelength shift between it and the standard star due to flexure. *Top*: Spectrum of the same star after correction for the wavelength shift. The telluric CH_4 line at 3.28 μm is almost totally opaque and so the signal-to-noise in its vicinity is poor. The object was observed at an air-mass of 1.10 and the standard at 1.13. Note that in the cleaner telluric region > 3.5 μm, flexure has no significant effect.

The quality of the corrected 3.0-3.4 μm data shown in Figure 8 is exceptional and required a dry night, and bright stars (*K*~6) observed close in air-mass. A more typical quality is mid-way between the two plots. Scientifically, the most productive long wavelength cross-dispersed modes have been the 1.9-4.2 μm, and 2.2-5.0 μm modes. These modes have the advantage of obtaining coverage of the *K*-band simultaneously with the *L* and *M*′-bands. The 3.5-4.2 μm and 4.6-4.8 μm regions are usually amenable to good telluric correction. There has been relatively little demand for the 2.4-5.4 μm cross-dispersed mode due to severe telluric problems at 5.0-5.4 μm.

5. MAINTENANCE ISSUES

As of May 2004 SpeX has been in use on the IRTF for four years. During this period it has averaged about 45% of all awarded telescope time for a total of about 650 12-hour shifts (usually nights). Over this time about 35 nights were lost, 15 nights due to instrument problems, and 20 nights due to a handling accident. Not including the handling accident, the instrument downtime is running at 2.5%.

Downtime for possible maintenance is scheduled for a few weeks each six-month observing semester. Occasional tasks include filter changes and closed-cycle cooler replacement. The 1050-CTI cooler used in SpeX was replaced after two years when its performance began a slow decline. A two-year life for closed-cycle coolers is typical at IRTF provided the helium gas and lines are kept free from contamination. SpeX was kept cold from the cooler replacement in January 2002 until the handling accident in April 2004.

The majority of the instrument problems have involved electronic board failures in the array controller. About half of these appear to be random failures but some are related to brown-outs and power outages at the telescope. The symptoms of a failure are usually a good indicator of which board has failed and this type of problem is usually fixed within a few hours of troubleshooting. A full set of spare boards is kept at the telescope. The cryo-mechanics have proved extremely robust. SpeX has seven cold mechanisms controlled by warm motors. Apart from a loose set screw in the feed-through to the K-mirror rotator, the mechanisms have been problem free. In April 2001 the spectrograph array suddenly developed increased gain and persistence in two quadrants. When no problems were found in the warm signal train, the array was removed and installed in lab dewar for testing. In the process a few flakes of aluminum were cleaned off the array fanout wires. The following cold tests were normal and the array was reinstalled in the SpeX without further incident. We suspect that the problem was caused by an aluminum flake shorting across two fanout wires.

The handling accident occurred in April 2004 when SpeX was moved from its off-axis stow position into the on-axis position for observing. Unfortunately, the telescope instrument rotator, to which all instruments bolt, was left with only one of its four brakes locked after use the previous night. When the telescope was slewed to the first star at the beginning of the next night, the rotator slipped, tensioning the shortest cable to the cryostat, before pulling off the cable connector's one-inch diameter vacuum seal. This resulted in a rapid loss of vacuum and exposed the cold arrays and cold optics to potentially damaging thermal shock as warm air rushed in. Some of the optical materials used in SpeX (CaF2, BaF2 and LiF) are notoriously susceptible to thermal shock. Remarkably both the arrays and optics survived unscathed and after three weeks for repairs and cleaning, SpeX was back in normal operation. The arrays themselves did receive a dusting and had to be removed and carefully cleaned. The pinning of all assemblies meant that the optical alignment was not disturbed. Inside the cryostat the arrays and optics are enclosed in light-tight aluminum cold boxes which are further protected by aluminum radiation shields, and so warm air entering the cryostat possibly undergoes significant cooling before reaching the arrays and optics, which might explain their survival.

7. LESSONS LEARNED

SpeX has proved to be a very productive instrument for the IRTF. In this section we will highlight a few areas where the instrument has exceeded expectations, and perhaps more interestingly, the areas where we have had problems. Work on SpeX started late 1994 and it was commissioned on the IRTF in June 2000, about 1.5 years late. The total cost to commissioning was about $2.1m compared to the projected cost of $1.4m at the start of the project. Funding was received from NSF ($1.25m) and the University of Hawaii ($0.15m in matching funds). Included in this was only $0.1m for detector arrays. However, SpeX received first pick of arrays (worth about $0.35m) from a foundry run funded independently by NASA (PI Dr. Mike Mumma). The cost overrun of $0.7m was funded from IRTF operations money. The reason for the late delivery of SpeX to the telescope was a combination of the late arrival of the arrays (in late 1999), and the late delivery of cryostat components from outside vendors.

The performance of the infrared slit-viewer for object acquisition, guiding and science imaging, has exceeded our expectations. In combination with the internal K-mirror image rotator it has increased significantly observing efficiency by simplifying object setup and guiding. The guider array and spectrograph array operate simultaneously with no

interference. Using a separate array for object acquisition, rather than the spectrograph array in an imaging mode as is done in some infrared spectrographs, avoids exposing the spectrograph array to higher flux levels than otherwise necessary. This became a significant issue when Aladdin arrays turned out to have higher levels of persistence than predicted, the effects of which were discussed in section 3.4.The use of a rotating turret in which gratings and cross-dispersing prisms are used in double-pass mode made it easy to in install new spectral modes (such as the low spectral resolution prism mode), to fine tune the rotation to bring other orders onto the spectrograph array (e.g. moving from 1.9-4.2 μm to 2.2-5.0 μm in the long wavelength mode), and to avoid areas of bad pixels without having to move the array. Only about ten nights were required to commission SpeX on IRTF. This was because of the six months of extensive all-up instrument testing in the lab (see Figure 9). Not surprisingly one area that required work was the interaction of the SpeX guider control software with the telescope which was not simulated in the lab.

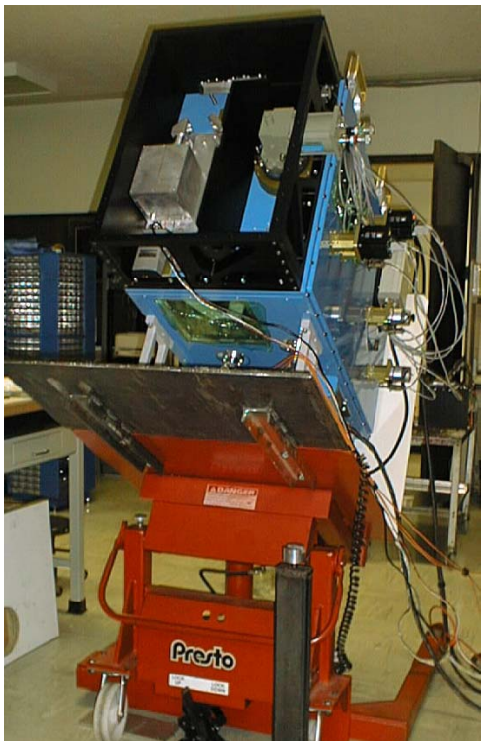

Figure 9 Flexure testing in the lab. The cryostat is shown tilted at 60 degrees. The closed-cycle cooler and calibration unit are visible at the top of the cryostat.

At about 500 Kg SpeX is about as big an instrument as can be reasonably mounted on the 3 m IRTF. The telescope counter-balance system had to be upgraded and the torque of the brakes on the cassegrain instrument rotator increased for SpeX to mount on the telescope. However, a more systems engineering approach to the project might have highlighted the risk of personnel neglecting to properly secure the rotator brakes which eventually led to the handling accident. SpeX contains its own K-mirror image rotator and so does not need to rotate. It was a very simple fix to attach lugs to the cryostat to prevent it from rotating. The amount of work required to write the *Spextool*[4] data reduction package was grossly underestimated and as a consequence *Spextool* was not available to observers until one year after instrument commissioning. The throughput below 1.2 μm is less than predicted (see Figure 7 in Rayner *et al*.[1]). We believe this is probably due to a combination of decreasing quantum efficiency of the array and decreasing efficiency of the 0.8-5.5 μm anti-reflection coatings towards shorter wavelengths. In general the custom gratings made for SpeX met efficiency predictions although the blaze profiles were shifted to slightly shorter wavelengths and were slightly narrower than expected. Flexure in SpeX is 1-2 pixels (depending on direction) at a tilt of 60 degrees. While this is good it did not meet the specification of 0.2 pixels predicted by finite element analysis (FEA) of the instrument. Measurements indicate that the source of the extra flexure is the optical mounts that were only modeled as simplified structures in the original FEA. As discussed in section 4.3, even flexure at the level of ~0.1 pixels can make it difficult to remove telluric features from spectra. The problem of persistence negated the good dark current performance of the Aladdin arrays. Finally, in future instruments we would seriously consider not mounting the arrays as upward looking as in SpeX, to avoid accumulating debris on the arrays and fanout wires, which has been at least a partial factor in the only two significant downtimes the instrument has experienced.

REFERENCES

1. Rayner, J.T., Toomey, D.W., Onaka. P.M., Denault, A.J., Stahlberger, W.E, Vacca, W.D., Cushing, M.C & Wang, S. 2003, PASP, 115, 362
2. Fowler, A.M. & Gatley, I. 1990, ApJ, 353, L33
3. Vacca, W.D., Cushing, M.C. & Rayner, J.T. 2004, PASP, 116, 352
4. Cushing, M.C., Vacca, W.D & Rayner, J.T. 2004, PASP 116, 362
5. Goto, M., Hayano, Y., Kobayashi, N., Terada, H., Pyo, T-S., Tokunaga, A.T., Takami, H., Takato, N, Minowa, Y., Gaessler, W. & Iye, M. 2003, Proc. SPIE, 4839, 1117
6. Vacca, W.D., Cushing, M.C. & Rayner, J.T. 2003, PASP, 115, 389